Electronic Supplementary Material (ESI) for Catalysis Science & Technology

One-pot synthesis of mesoporous ZrPW solid-acid catalyst for liquid phase benzylation of anisole

Zhichao Miao[a,b], Huanling Song[a,c], Huahua Zhao[a], Leilei Xu[a,b], Lingjun Chou[a,c*]

[a] State Key Laboratory for Oxo Synthesis and Selective Oxidation, Lanzhou Institute of Chemical Physics, Chinese Academy of Sciences, Lanzhou 730000, People's Republic of China.

[b] University of Chinese Academy of Sciences, Beijing 100049, People's Republic of China.

[c] Suzhou Institute of Nano-Tech and Nano-Bionics, Chinese Academy of Sciences, Suzhou 215123, People's Republic of China.

[*] Corresponding author: e-mail: **ljchou@licp.cas.cn** (L. J. Chou)
Tel: +86 0931 4968066; Fax: +86 0931 4968129

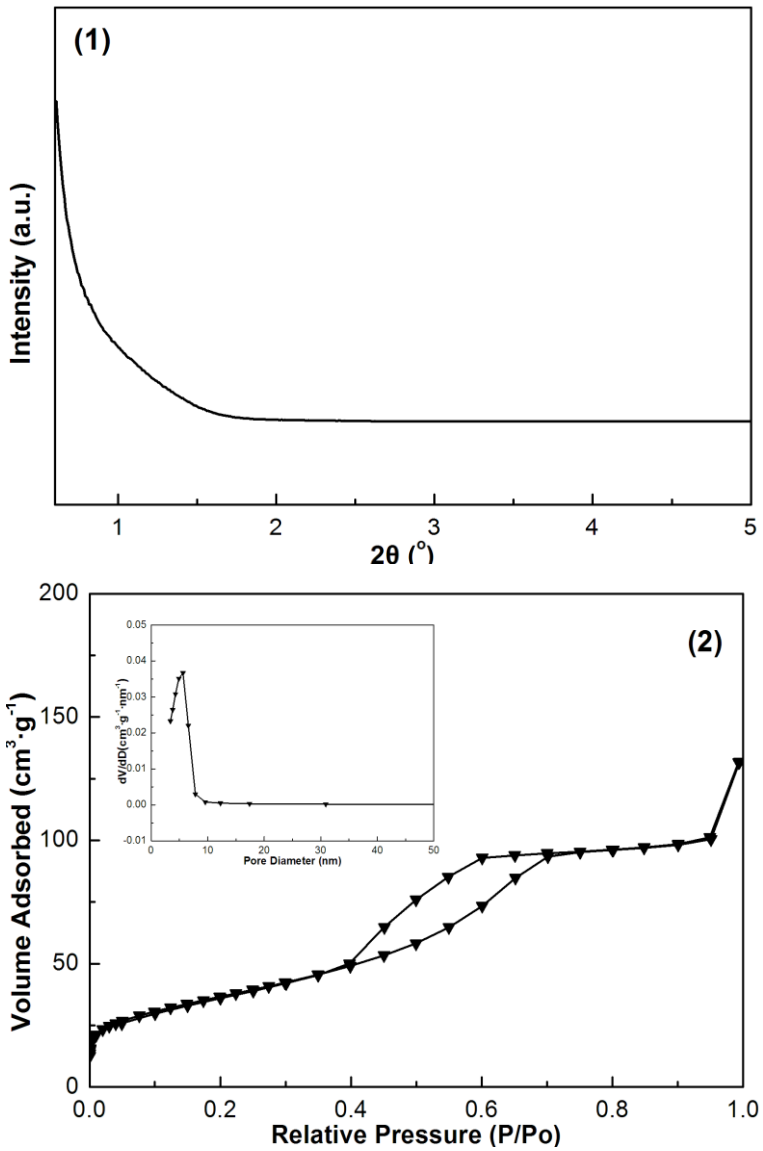

Figure S1. Small-angle X-ray diffraction **(1)**, isotherms **(2)** and pore size distributions **(inset of (2))** of the M-ZrPW-25

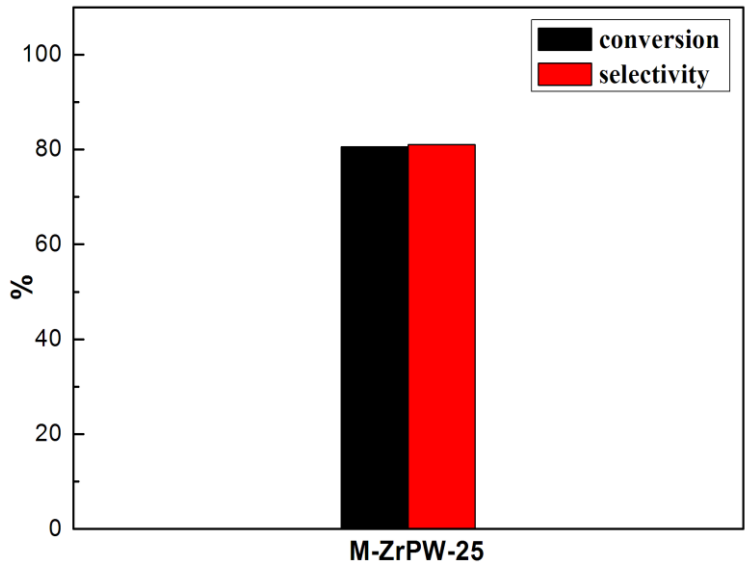

Figure S2. Friedel-Crafts benzylation reaction catalyzed by M-ZrPW-25

We employed SXRD and N_2-physisorption to characterize the gotten M-ZrPW-25. As shown in Fig. S1(1), the M-ZrPW-25 showed no diffraction peaks in the SXRD patterns, indicating the absence of ordered mesostructure in the sample. In addition, nitrogen adsorption and desorption isotherms (Fig. S1(2)) of the sample showed typical H2 shaped hysteresis loops rather than H1 shaped hysteresis loops, indicating the pore structure had deformed with the introduction of excess tungsten species. The textural properties of M-ZrPW-25 were shown in Table S1. The specific surface area, pore size and volume decreased largely in the sample. Therefore, the formation of excellent mesostructure in M-ZrPW-25 was restricted.

In addition, the catalytic performance of M-ZrPW-25 was investigated. As shown in Fig. S2, the catalytic activity began to decrease when the tungsten species increased to 25% and only showed 80.6% conversion and 81% selectivity in M-ZrPW-25. We deduced this might be mainly due to the decrease of the specific surface area and the active sites for the reactant.

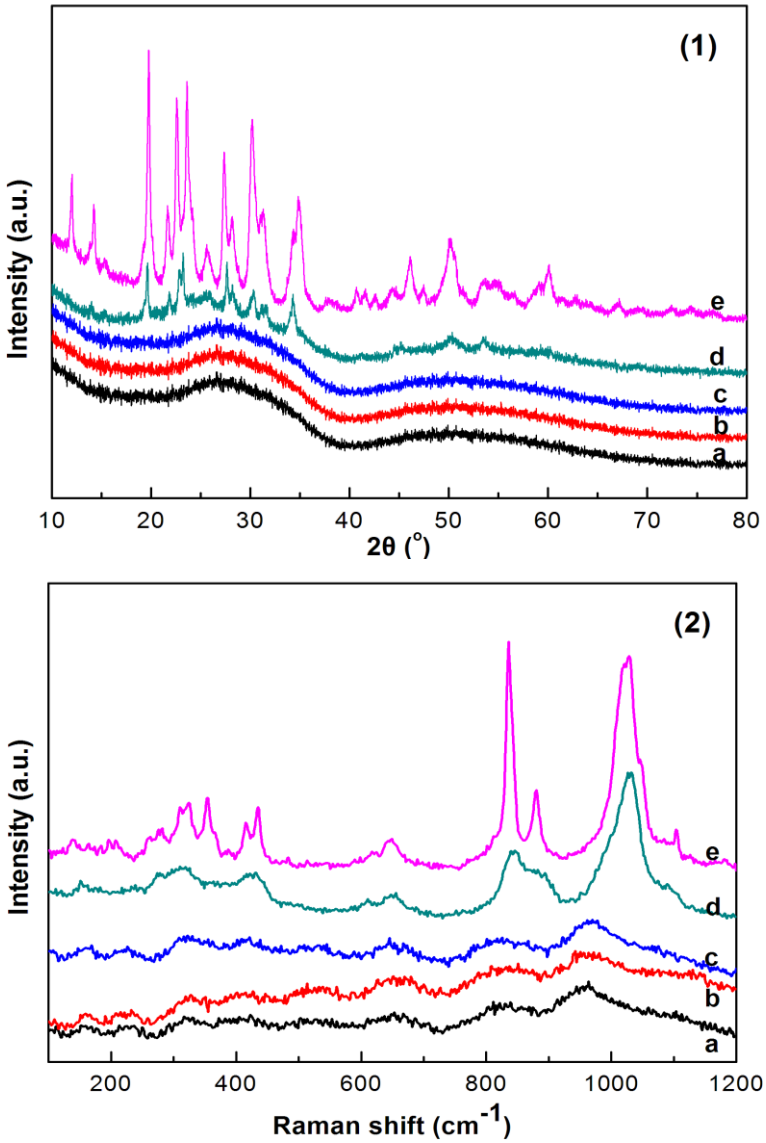

Figure S3. Wide-angle X-ray diffraction patterns **(1)** and Raman spectra **(2)** of M-ZrPW-20 treated at different temperature: **(a)** 500 °C, **(b)** 600 °C, **(c)** 700 °C, **(d)** 800 °C,**(e)** 900 °C.

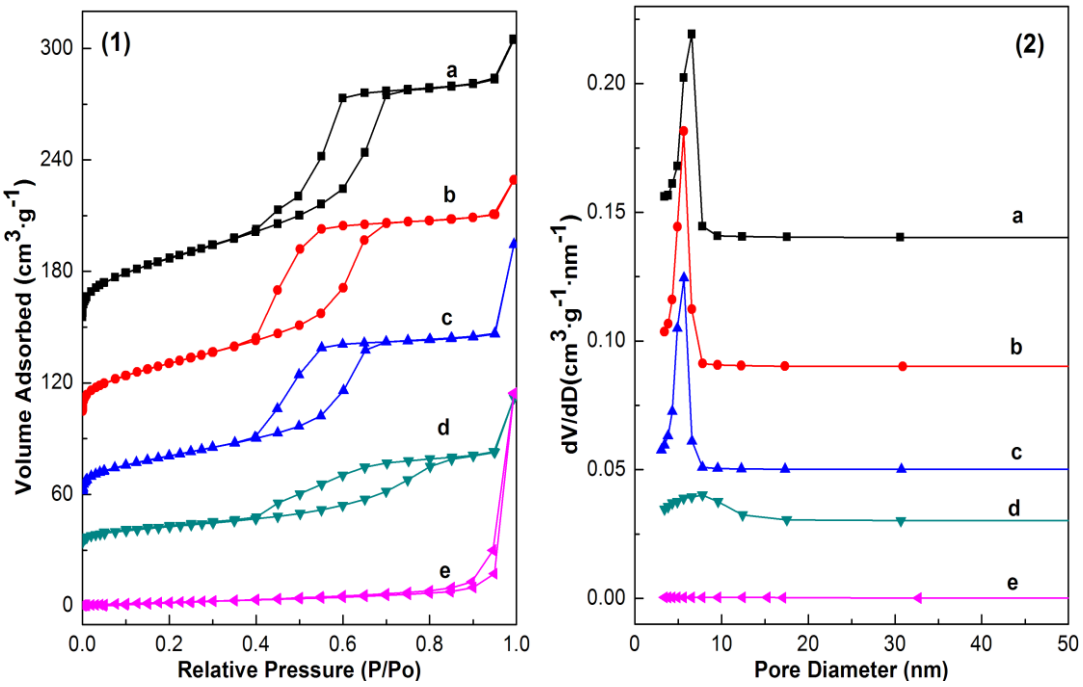

Figure S4. Isotherms **(1)** and pore size distributions **(2)** of M-ZrPW-20 treated at different temperature: **(a)** 500 ^{o}C, **(b)** 600 ^{o}C, **(c)** 700 ^{o}C, **(d)** 800 ^{o}C,**(e)** 900 ^{o}C.

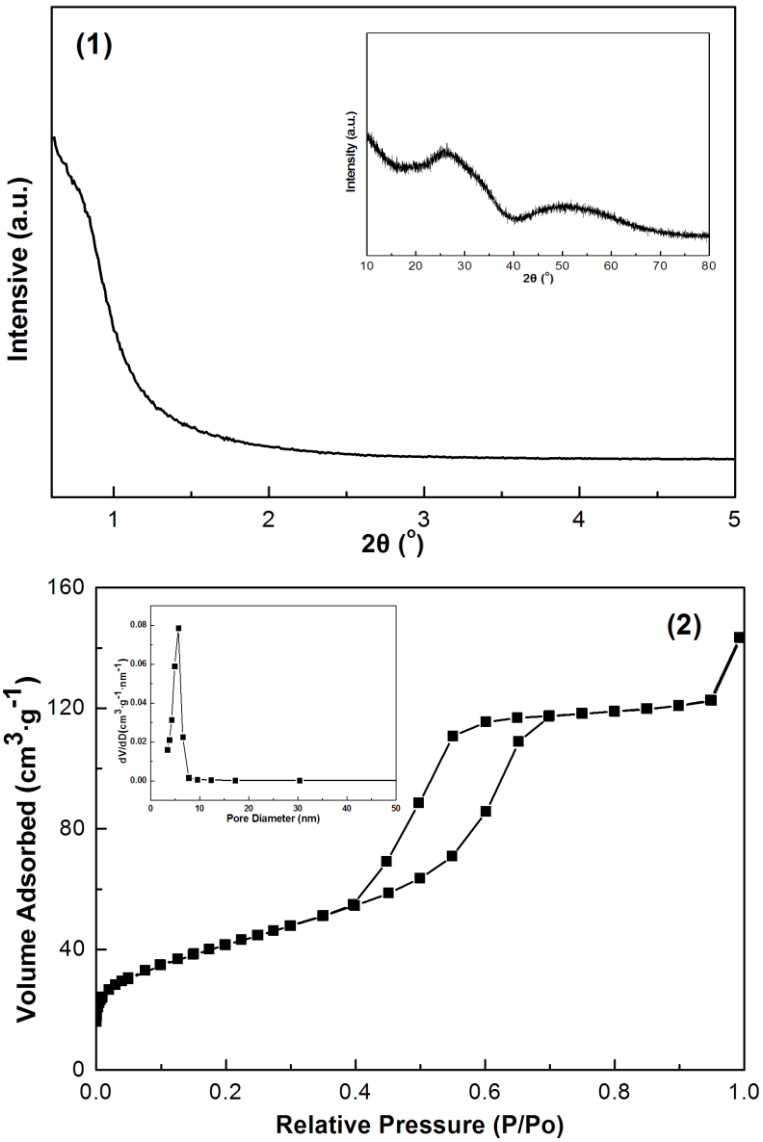

Figure S5. Small-angle X-ray diffraction **(1)** and Wide-angle X-ray diffraction **(inset of (1))** patterns, isotherms **(2)** and pore size distributions **(inset of (2))** of the used catalyst M-ZrPW-20.

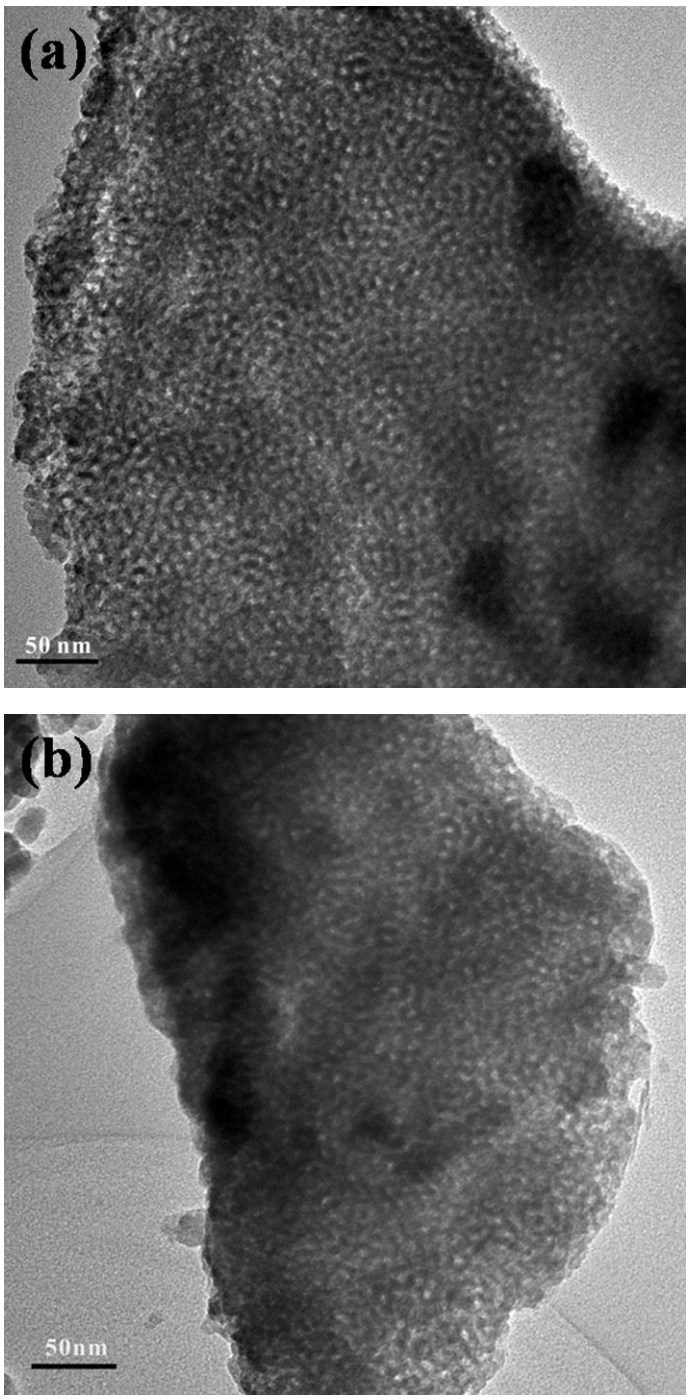

Figure S6. TEM images of the used catalyst M-ZrPW-20 after five cycles.

Table S1. Textural properties of the M-ZrPW-25, M-ZrPW-20 treated at different temperature, the used M-ZrPW-20 derived from Nitrogen adsorption and desorption Data.

Samples	Calcination Temperature	Nitrogen adsorption and desorption Data		
		Specific Surface Area ($m^2 \cdot g^{-1}$)	Pore Size (nm)	Pore Volume ($cm^3 \cdot g^{-1}$)
M-ZrPW-25-500	500	129.2	5.60	0.14
M-ZrPW-20-500	500	168.3	6.26	0.23
M-ZrPW-20-600	600	144.5	5.62	0.20
M-ZrPW-20-700	700	109.5	5.64	0.17
M-ZrPW-20-800	800	45.9	7.79	0.10
M-ZrPW-20-900	900	10.1	—	—
M-ZrPW-20-used	500	148.8	5.65	0.21